ACS Energy LETTERS

http://pubs.acs.org/journal/aelccp

Letter

Thermoformable Electrolytes for Solid-State Sodium Metal Batteries Employing Organic Cathodes

Dong-Min Kim, Gan Chen, Michael A. Baird, Livia Pugens Matte, Youngmin Ko, Carson O. Zellmann-Parrotta, Jiwoong Bae, Zhaoyang Chen, Yan Yao, Mary C. Scott, Ying Chen, and Brett A. Helms*

Cite This: https://doi.org/10.1021/acsenergylett.6c00026

Read Online

ACCESS | Metrics & More | Article Recommendations | Supporting Information

Downloaded via UNIV OF HOUSTON MAIN on January 31, 2026 at 23:01:35 (UTC).
See https://pubs.acs.org/sharingguidelines for options on how to legitimately share published articles.

ABSTRACT: Solid-state sodium metal batteries (SSBs) are candidates for TWh-scale energy storage systems, yet remain challenged by poor processability, cracking, and interface incoherence between inorganic electrolytes and cathodes. Here, we architect thermoformable organo−ionic (ORION) electrolytes comprising controllably clustered ion aggregates within a zwitterionic matrix to create SSBs with organic cathodes. ORION electrolytes are viscoelastic liquids above 110 °C, yet they are viscoelastic solids at typical battery operating temperatures, which overcome the aforementioned challenges. We introduced ether ligands to tailor Na^+-ion coordination environments and transport over 3 orders of magnitude (3.4×10^{-3} − 1.0 mS cm^{-1}), whereupon we observed monotonic increases in Na^+ mobility with increasing coordination number (up to 2.5); yet the fraction of mobile ions decreased. Thus, ligands dissociate Na^+ from larger ion clusters and aggregates, prescribe what the effective mass of Na^+ will be, and how Na^+ will move within the zwitterionic matrix via vehicular diffusion.

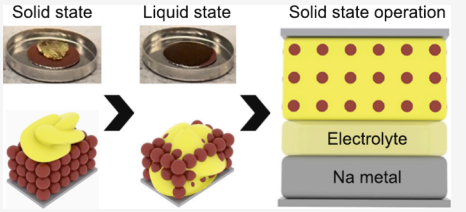

Solid-state sodium metal batteries (SSBs) are promising candidates for TWh-scale energy storage systems,[1−5] however, their development has been constrained by ongoing challenges in interfacing inorganic solid electrolytes and cathodes and retaining those interfaces during cycling.[6−9] To create inorganic−inorganic interfaces in separators and cathodes, high temperature[10−14] and pressure[15−18] are required, which also serve to densify the components, yet such processes can lead to undesirable interdiffusion,[19−21] phase changes,[22−24] or mechanical mismatches[25−27] that compromise interfacial stability upon cooling or over time as the battery is cycled. Alternative strategies invoking organic−organic interfaces in solid-state batteries offer more direct routes to conformal interfaces at low temperature and pressure, e.g., if enabled by dynamic bonding such as ion pairing or other supramolecular associations.[28,29]

Here, we describe SSBs comprising thermoformable organo−ionic (ORION) viscoelastic solid electrolytes and organic cathodes, streamlining cell fabrication and lowering the metal burden for cell manufacturing at scale. ORION electrolytes implement organic zwitterionic supramolecular building units (SBUs) that act as a high-dielectric networking agent for sodium salts and their accompanying Na^+-binding ligands: 1,2-dimethoxyethane (G1) or 1-methoxy-2-(2-methoxyethoxy)ethane (G2). Within this design space, we restrict the number of Na^+-coordinating oxygen functionality in the ligands to be less than or equal to the total number of available coordination sites at Na^+, which ensures little to no free ligand in these viscoelastic coordination solids. This constraint distinguishes ORION electrolytes from ion-conducting gels and often allows battery operation outside the thermodynamic stability window of ethereal organic ligands.[30−32] Introducing ligands in this manner lowers the glass transition temperature (T_g) by as much as 133 °C, i.e., from 65 °C to −68 °C. With specific combinations of SBU, sodium salts, and ethereal ligands, we demonstrated an ionic conductivity of up to 1.0 mS cm^{-1} at 70 °C. The higher mobility of Na^+ ions with increasing ligand concentration was further supported by nuclear magnetic resonance (NMR) measurements, yet we surprisingly found that the ratio of structural vs mobile Na^+ was largely unchanged: 40% structural vs 60% mobile. When assembling SSBs, we leveraged the thermoformability of ORION electrolytes to create conformal interfaces within the electrodes (Figure 1a). At low stack pressure and low temperature (i.e., coin cells), we measured a critical current density in Na|ORION|Na cells of ∼0.15 mA cm^{-2}; Na-metal plating and stripping were reversible and stable over 400 cycles. We further observed stable cycling over at least 200 cycles for Na|ORION|cathode cells cycled at moderate current density, inviting further exploration of all-

Received: January 5, 2026
Accepted: January 20, 2026

© XXXX American Chemical Society

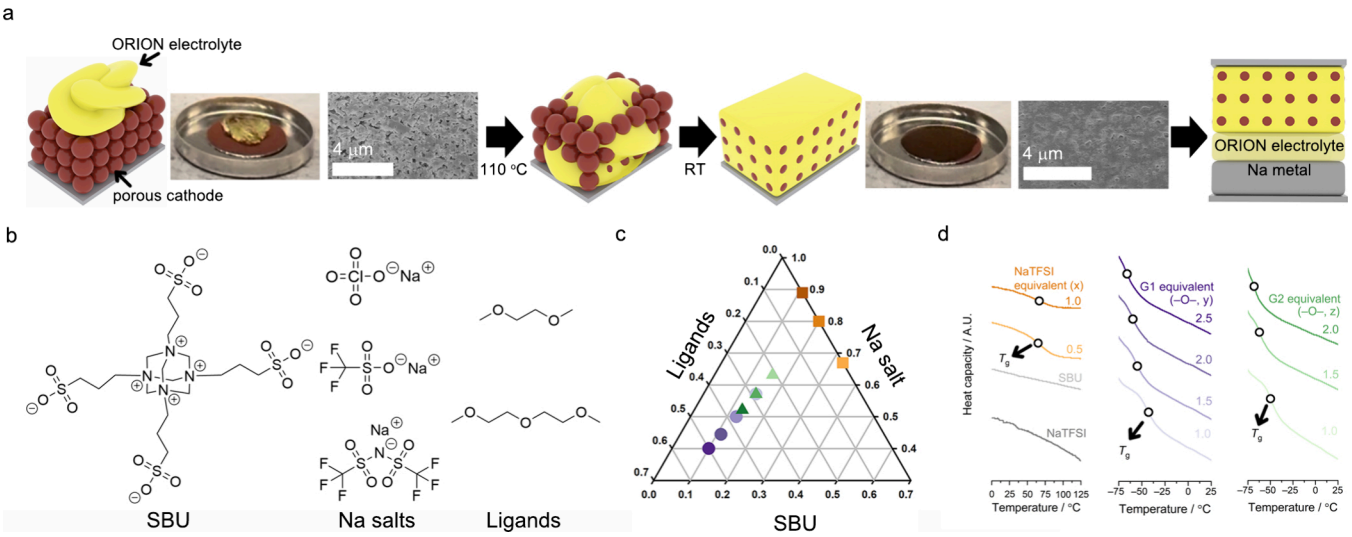

Figure 1. (a) Schematic, demonstration, and FIB-SEM images of thermoformability of ORION electrolytes, shown by their unassisted infiltration into the pores of composite electrodes comprising organic active materials. (b) Design space considered here, where a zwitterionic structural building unit (SBU) serves as host to sodium salts and optionally Na^+-coordinating ethereal organic ligands. (c) Ternary phase diagram and electrolyte compositions considered, wherein compositions are presented as molar fractions of SBU, NaTFSI, and ether ligand. (d) Glass transition temperatures (T_g) of ORION electrolytes (orange: ORION electrolyte composed of SBU and NaTFSI, purple: ORION electrolyte composed of SBU, NaTFSI and G1, green: ORION electrolyte composed of SBU, NaTFSI and G2; compositions are represented as either SBU(SO_3^-):NaTFSI (x) or SBU (SO_3^-):NaTFSI:Ligand (−O−, G1 (y), or G2 (z)) = 1:1:y or z), depending on whether an ether ligand is introduced.

organic solid state sodium metal batteries for emerging energy storage applications.

Our findings complement a growing body of foundational work on concentrated liquid electrolytes, which chart new opportunities for ion conductors in sodium-ion and sodium−metal batteries.[30,33−35] While we draw inspiration from this design space,[32,36,37] we bring new insights by introducing small-molecule zwitterionic structural building units, which transform concentrated liquid electrolytes into viscoelastic solids with broadly tunable properties. Within this context, we quantify the impacts of the emergent coordination chemistry on structure, dynamics, and transport, providing in situ examples of their applicability in all-organic solid-state sodium metal cells operating under low stack pressure. With these first insights and demonstrations, we anticipate that future interest and intrigue will be in comparing solid-state battery behaviors across various all-organic or all-inorganic chemistries; this work seeds the growth of those efforts.

To produce Na ORION electrolytes, we combined the zwitterionic SBU[28] with a Na salt (e.g., sodium perchlorate ($NaClO_4$), sodium trifluoromethanesulfonate (NaOTf), or sodium trifluoromethanesulfonimide (NaTFSI))—and an ethereal ligand (G1 or G2) (Figure 1b) and heated the mixture. This process yielded homogeneous viscoelastic liquids at elevated temperature, when salt solubility is high; it produced unusable heterogeneous mixtures, when salt solubility was too low. We will describe herein the composition of various ORION conductors based on the number of equivalents of SO_3^- groups from SBU (each SBU provides four $-SO_3^-$ moieties) relative to the number of equivalents of Na^+ ions originating from the sodium salt (each salt molecule provides one Na^+) and the number of equivalents of Na^+-binding oxygen atoms from the ethereal ligands (G1 contributes up to two L-type coordinating oxygen atoms; G2 contributes up to three per molecule).

We initially examined the dissolution behavior of various Na salts with the zwitterionic SBU in the absence of an ethereal ligand using differential scanning calorimetry (DSC), as shown in Figure S1. Each Na salt was mixed with SBU in a SBU(SO_3^-):Na^+ = 1.0:1.0 ratio. Among the Na salts, only NaTFSI exhibited complete dissolution at these high concentrations: the onset of the endothermic peak for NaTFSI was ∼110 °C, while no endothermic peaks were evidenced for the other salts. Mixtures of NaTFSI and SBU remained homogeneous after being cooled (Figure S1). By using X-ray diffraction (XRD) (Figure S2), we confirmed that after heat treatment, ORION conductors with SBU(SO_3^-) to NaTFSI ratios of 1.0:0.5 and 1.0:1.0 were amorphous, indicating highly effective salt dissolution. With ratios of SBU(SO_3^-):NaTFSI = 1.0:2.0, diffraction peaks characteristic of NaTFSI reappeared, which suggested the solubility limit of NaTFSI in SBU(SO_3^-) to be approximately 1.0:1.0 ratio.

We next introduced either G1 or G2 ethereal ligands in prescribed amounts to the concentrated amorphous organo−ionic matrix comprising zwitterionic SBU and NaTFSI. (Figure 1c). We anticipated that the addition of ethereal ligands would function to reduce the T_g, as they are typical declustering agents in concentrated electrolytes, where they act to lower the prevalence of complex aggregates (AGG) and contact ion-pairs (CIP) in favor of ligand-separated ion-pairs (LSIP). Specific ORION electrolyte compositions made with different ether ligand ratios, i.e., SBU(SO_3^-):NaTFSI: G1(−O−) or G2(−O−) = 1.0:1.0:y or z, where y = oxygen ratio from G1 and z = oxygen ratio from G2), will be referred to hereafter simply as "y G1" or "z G2". As shown in Figure S3, for compositions with an oxygen (from ligand) ratio to sodium lower than 2.5 G1 and 2.0 G2, the ORION conductors remained homogeneous solids at room temperature. However, compositions with ligand ratios exceeding these thresholds became inhomogeneous, indicating the bounds by which ether ligands should be implemented. Within the allowable homogeneous regime, the compositions were viscoelastic liquids above 110 °C, while returning to viscoelastic solids when cooled, enabling the infiltration of ORION electrolyte in

https://doi.org/10.1021/acsenergylett.6c00026
ACS Energy Lett. XXXX, XXX, XXX−XXX

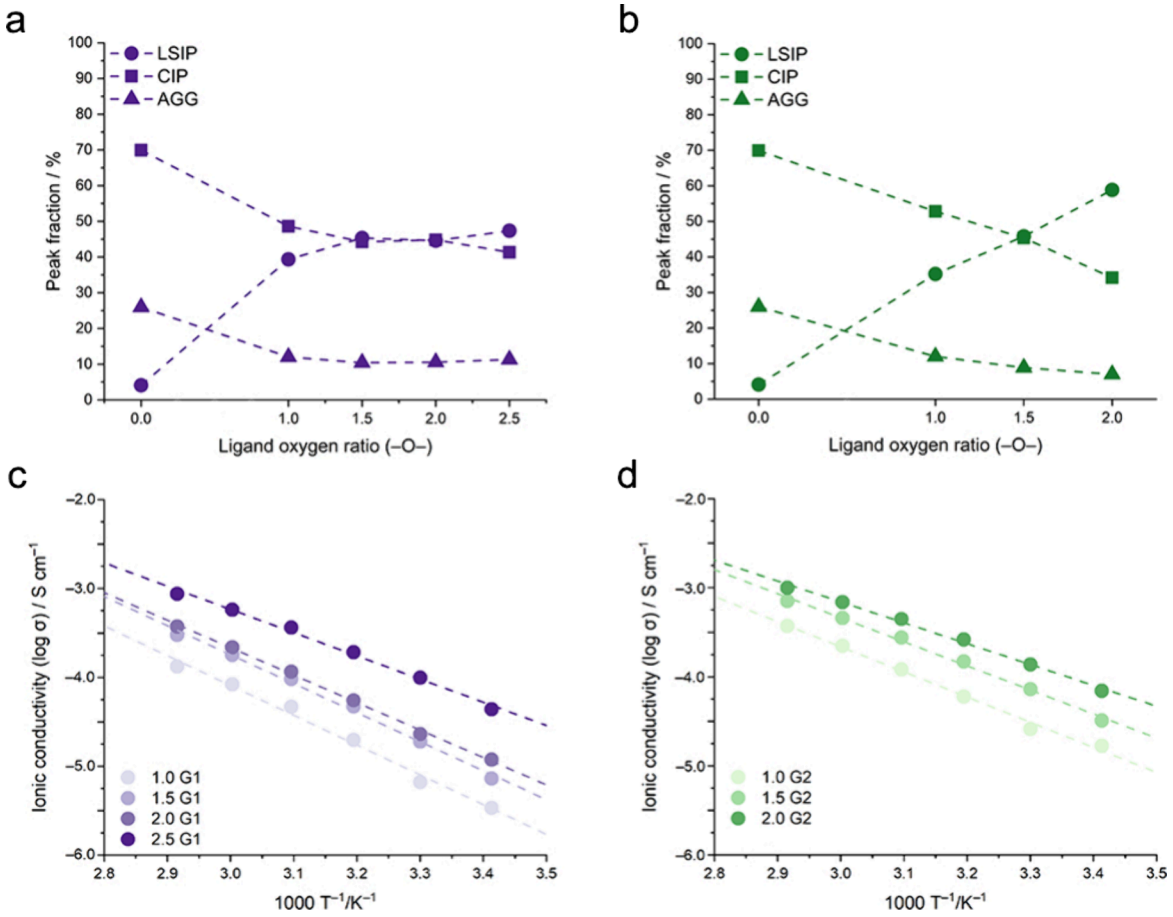

Figure 2. Coordination chemistry of (a) G1-based and (b) G2-based ORION viscoelastic solid electrolytes deconvoluted from Raman spectra and (c, d) ionic conductivity of ORION viscoelastic solid electrolytes, calculated from electrochemical impedance spectroscopy of the materials with different amounts of ether ligands.

composite cathode. FIB-SEM analysis (Figure 1a) and photos (Figure S4) confirmed effective infiltration using this thermal process.

While NaTFSI-based ORION electrolytes obviating an ether ligand had a glass transition temperature (T_g) of 65 °C, addition of either G1 or G2 ligands lowered it to as low as T_g = −68 °C. Collectively across the series, T_g values of ORION electrolytes were lowered to the range of −43 to −63 °C when G1 was used as the ligand and −50 to −68 °C when G2 was used. Furthermore, T_g changed monotonically with the ether ligand ratio, indicating that the physical properties of the Na ORION electrolyte can be modulated by adjusting the ether ligand ratio (Figure 1d, Figure S6)

The dramatic decrease in T_g with relatively few ethereal ligands in the ORION conductors motivated a deeper investigation of their solid-state coordination chemistry by Raman spectroscopy. We deconvoluted the spectra (Figure S7), focusing our attention on AGG, CIP, and LSIP features as reported by the $TFSI^-$ anion (Figure 2a,b).[30,38] Unsurprisingly, the ORION conductors obviating ethereal ligands were dominated by AGG and CIP features in the solid-state. In stark contrast, with increasing amounts of either G1 or G2, LSIP emerged as dominant, at the expense of AGG and CIP. Interestingly, regardless of the choice of ether ligand, the percentage of AGG rapidly dropped at the lowest ligand amount used and did not change substantially thereafter as more ligand was introduced. On the other hand, the effects of introducing larger amounts of ligand was primarily affecting the balance of CIP and LSIP. More specifically, to increase the percentage of LSIP in the ORION conductors required additional G1 or G2 ligand, yet, the specific choice of G1 or G2 governs the rate of change of increase in LSIP over other species. Higher percentages of LSIP (∼40%) are immediately available at low ligand ratios for G2 and the highest percentage at the largest ligand amount used was ∼60%. Introducing increasing amounts of G2 produced less of a stepchange, by comparison to G1, but reached the highest percentage of LSIP in the series we considered (∼60%). This suggested that G2 has a stronger declustering effect, which could facilitate Na^+ conduction.

We quantified the extent of ligand-enhanced Na^+-ion conduction in ORION electrolytes across the series through electrochemical impedance spectroscopy (EIS) in cells implementing stainless-steel blocking electrodes (Figure S8) and therefrom ionic conductivity determinations (Figure 2c,d). For G1 ligands, the ionic conductivity of the 1.0 G1 ORION electrolyte increased from 3.4×10^{-6} S cm^{-1} (1.0 G1, 20 °C) to 4.4×10^{-5} S cm^{-1} (2.5 G1, 20 °C) with higher ligand content. The same trend was also observed for G2 ligands, increasing from 1.7×10^{-5} S cm^{-1} (1.0 G2, 20 °C) to 6.9×10^{-5} S cm^{-1} (2.0 G2, 20 °C). These results indicate that both ligands effectively promoted the Na^+ mobility. Furthermore, comparing G1 vs G2 ligands, ORION electrolytes with G2 exhibited higher ionic conductivity than with G1 when the

https://doi.org/10.1021/acsenergylett.6c00026
ACS Energy Lett. XXXX, XXX, XXX−XXX

same number of L-type oxygens were available in the system, supporting the conclusion that G2 is a stronger declustering ligand than G1. This trend was observed across the entire temperature range considered (20−70 °C). Notably, among all the Na ORION electrolytes tested, 2.0 G2 achieved the highest ionic conductivity of 1.0 mS cm^{-1} at 70 °C, corresponding to the largest LSIP coordination fraction in Figure 2b.

To understand whether ions move more freely in ORION conductors with G2, we modeled the temperature-dependent conductivity data, determining the activation energy (E_a) (Figure 2c,d), using the Arrhenius equation below: σ, σ_0, k_B, and T denote ionic conductivity, pre-exponential factor, Boltzmann constant, and temperature (K), respectively.

$$\sigma = \sigma_0 e^{-E_a/k_B T}$$

This analysis shows that G1 reduces E_a from 0.67 to 0.51 eV over the range of stoichiometries considered here, while G2 reduces E_a from 0.56 to 0.47 eV (Table 1). These data further

Table 1. Calculated Activation Energy (E_a) from Figure 2c,d

ether ligand ratio (G1 or G2, −O−)	G1 (E_a, eV)	G2 (E_a, eV)
1.0	0.67	0.56
1.5	0.65	0.54
2.0	0.61	0.47
2.5	0.51	

support the notion that G2 is a superior declustering agent with accompanying benefits to ion transport. Because G2-based ORION electrolytes exhibited lower activation energies and higher ionic conductivity across compositions with same molar fraction of oxygen relative to Na^+, the data point to an intriguing and nonintuitive interplay of ligand design, spatial arrangement vis-à-vis network vs mobile ionic species, and ion dynamics in the underlying transport outcomes for these networked coordination solids.[30,32]

These insights into solid-state coordination chemistry, ionic conductivity, and activation barriers to ion motion beg follow-up questions as to the molecular origins of the properties of the ORION conductors: specifically, what fraction of Na^+ ions in the system are mobile; what fraction are structural; and how do the ligands affect those outcomes. We revisited the characterization of local coordination environments in ORION electrolytes by NMR, seeking to distinguish species on the basis of their dynamics. We examined ORION electrolytes with (1.0 G1) and without ligand for solid-state NMR measurements, as these are the stiffest solids and make magic angle spinning (MAS) possible. Without an ethereal ligand, we observed a broad signal with a shoulder between −10 and −15 ppm in the ^{23}Na magic angle spinning (MAS) spectrum (Figure 3a). ^{23}Na multiple quantum MAS (MQMAS) confirmed this shoulder originates from unincorporated Na^+ in crystalline NaTFSI, accounting for 4−5% of total Na^+ (Figure 3b and Figure S9). The broad signal between −1 and −18 ppm corresponded to a wide distribution of Na^+ mixed with SBU. Upon addition of ether (1.0 G1), the crystalline NaTFSI phase disappears, and a relatively sharper ^{23}Na signal centered around −10 ppm emerged alongside the broad component (Figure 3a,c). This sharper feature also appeared in the ^{19}F NMR spectrum of the 1.0 G1 Na ORION electrolyte (Figure 3d). When the second set of spinning sidebands was normalized to match that of the Na ORION electrolyte without a ligand, the additional sharper component in the central signal and the first set of sidebands confirmed its enhanced mobility. The "solid−like (structural)" and "liquid−like (mobile)" nature of the two Na^+ environments are further supported by the ^{23}Na nutation curve (Figure S10). The broader component exhibits a nutation frequency twice that of the sharper one, which matches that of fully coordinated Na^+. This indicates that the sharper signal originates from mobile Na^+ with a small quadrupolar coupling, while the broader signal arises from the central transition of structural Na^+ with a large quadrupolar coupling constant (≫20 kHz). Overall, ^{23}Na and ^{19}F NMR results confirmed the coexistence of relatively mobile Na^+ ions coordinated more by L-type ether ligands (50 ± 10%) and relatively rigid species interacting more strongly with X-type oxy-anions in the SBU (50 ± 10%).

More specifically, NMR signals from each ORION electrolyte formulation were deconvoluted (Figure S11) and the fraction of structural and mobile Na^+ was calculated (Table S1), using a multiplying factor described in the Supporting Information. Interestingly, they showed increasing percentages of structural Na^+ with increasing molar equivalents of L-type coordinating oxygen functionality in both G1 and G2. In this regime, we view the growth of the "structural Na^+" population not as immobilizing barriers, but as part of a reorganized coordination framework that smooths the energy landscape and facilitates faster motion of mobile Na^+ through dynamically exchanging Na−O coordination environments.

In short, there are principally two types of structural Na^+ in coordination solids: the first type is an electrostatic cross-link, where two sulfonate anions from the SBU are bound to Na^+; the second type is an electrostatic termination, where only one sulfonate anion is bound to Na^+, either as a contact-ion pair or a solvent-separated ion pair. Exchange dynamics, corresponding to the process by which free Na^+ exchanges with either of these species, is much more favorable for the latter. As more ligand is introduced, the fraction of electrostatic cross-links decreases with more terminal Na^+-associated species prevailing. The ionic conductivity benefits jointly from the lower cross-linking density and the higher fraction of network terminations, particularly when their exchange dynamics with mobile charge carriers are fast. Taken together, these observations showcase the importance of carrier mobility over carrier concentration in these emerging classes of viscoelastic solid electrolytes.

Temperature-dependent ^{23}Na NMR (Figure 3e) showed that, as the temperature rises from 5 to 65 °C, the broad component fades, while the initially sharp signal broadens. Two effects account for this behavior: (i) increased ionic mobility at a higher temperature and (ii) accelerated exchange between the two Na^+ environments. Without exchange, both resonances would narrow with increasing temperature, solely reflecting faster motion. Instead, the distinct signals observed at 5−25 °C coalesce into a single resonance at 55−65 °C, indicating that the exchange rate is the millisecond time scale within this temperature window. As the ether content increases from 1.0 to 2.5 G1 or 1.0 to 2.0 G2, the mobile Na^+ fraction decreased from 58.86 to 48.80% or from 58.27 to 53.81% (Figure S11, Table S1). Nevertheless, the sharp ^{23}Na resonance shifts steadily to higher frequency and its line width narrows, indicating that Na^+ ions become increasingly ligated by ethers and Na^+-ion mobility increases concomitantly (Figure 3f). This view provides unprecedented clarity on the foundations of ion transport in ORION conductors. Regarding the Raman analyses in Figure 2a,b, small amounts of Na^+-

https://doi.org/10.1021/acsenergylett.6c00026
ACS Energy Lett. XXXX, XXX, XXX−XXX

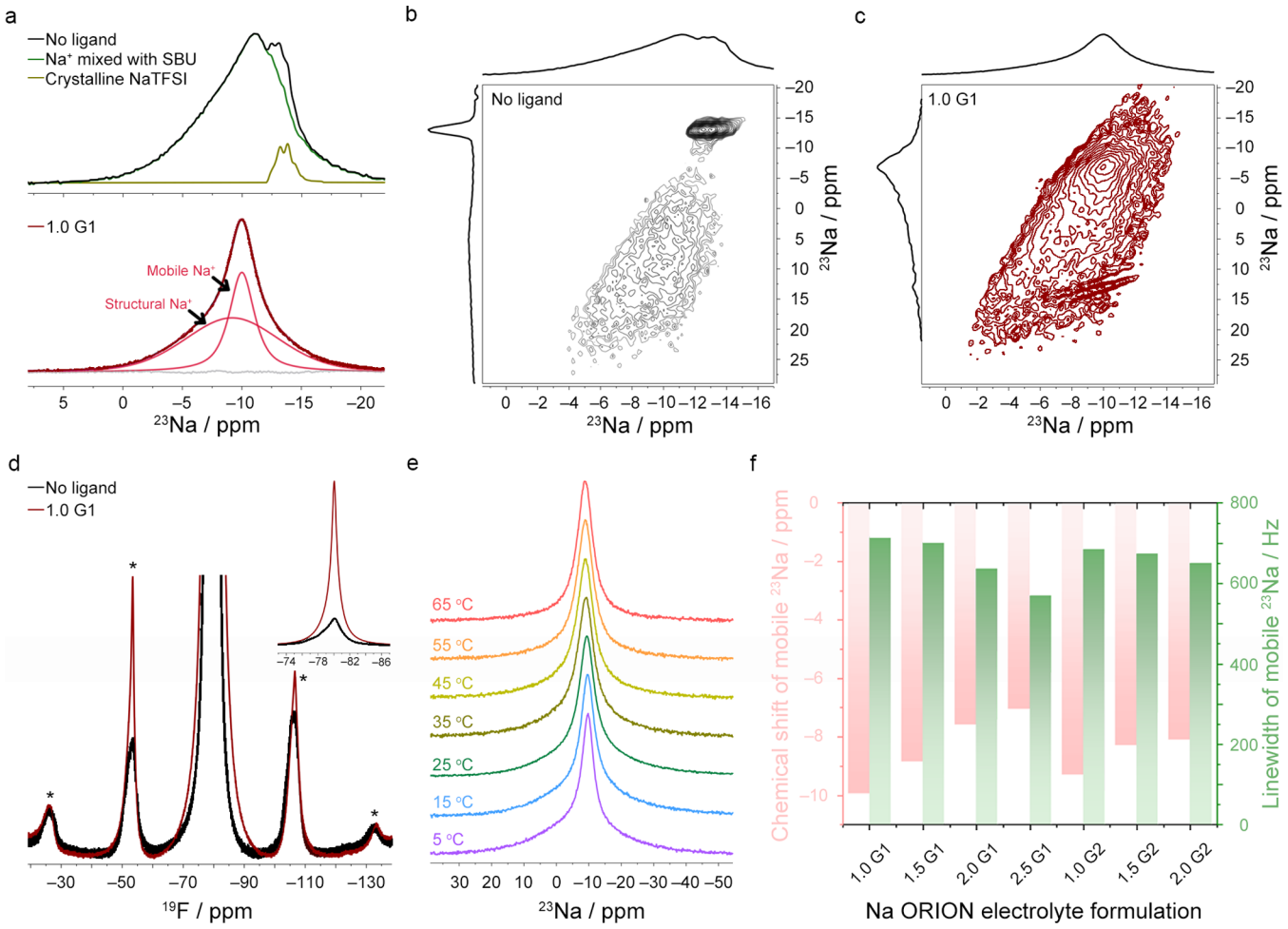

Figure 3. (a) Solid-state ^{23}Na MAS and (b, c) MQMAS spectra of Na ORION electrolytes without ligand or 1.0 G1. Spectra were acquired with a 9° pulse calibrated for the liquid-like (mobile) Na^+ resonance (equivalent to an 18° pulse for the solidlike (structural) component). Relative populations were obtained by spectral deconvolution and corrected to their respective 90° pulse widths for accurate comparison. (d) Solid-state ^{19}F MAS spectra of Na ORION electrolyte without ligand (black) and 1.0 G1 (red); asterisks denote the spinning sidebands. All solid-state NMR experiments were acquired at a spinning speed of 15 kHz. (e) Solution ^{23}Na NMR of the 1.0 G2 Na ORION electrolyte at varying temperatures. (f) ^{23}Na chemical shift and line width of mobile Na^+ of Na ORION electrolyte with different formulations.

coordinating ligands dramatically lower the fraction of ion clusters and aggregates in ORION conductors and substantially increase the fraction of ligand-separated ion pairs. With increasing amounts of ethereal ligands (yet staying below or equal to the total number of available coordination sites at Na^+), the fraction of mobile Na^+ decreases, and the ease in which those ions move through the matrix is improved, evidenced by the increasingly lower activation energies. This is surprising on several fronts, but most peculiar in the conclusion that adding more ethereal ligands does not substantially change the characteristics of mobile ions, but instead their interactions with the matrix.

The electrochemical behaviors of the 2.0 G2 ORION electrolyte were subsequently evaluated at 60 °C, focusing on both Na symmetric cell behavior and full-cell operation. Choice of cell operation temperature was informed by examining the accessible capacity and cell stability across a temperature range of 40−65 °C (Figure S12). In solid-state Na|ORION electrolyte|Na symmetric cells, we evaluated both interfacial stability and dendrite suppression in critical current density (CCD) tests and galvanostatic Na plating and stripping. When the current density was higher than 0.15 mA cm^{-2}, the Na stripping potential exhibited a spike at the end of the voltage profile, thus identifying it as the CCD (Figure 4a). We then operated the Na symmetric cells galvanostatically with a current density of 0.15 mA cm^{-2}, implementing a sequence of 1 h Na-metal plating/stripping cycles, whereupon the cells exhibited stable cycling profiles for over 400 cycles (Figure 4b), without signs of short circuiting or voltage instability. This long-term stability underscored both interfacial compatibility and favorable ion-transport properties of the ORION electrolyte, which was further corroborated by monitoring a low initial impedance as well as shallow impedance growth during the measurements across cycles (Figure S13). Origins of the increasing polarization in symmetric cell cycling was deconvoluted from EIS spectra taken every 20 cycles to delineate the respective influence of SEI resistance, bulk resistance of the ORION solid electrolyte, and charge-transfer resistance over time (Figure S14).

To further evaluate ORION electrolyte applicability in SSBs, we evaluated the electrochemical stability using a stainless steel electrode (Figure S15); the electrolyte was stable below 3.2 V. Based on this, we chose perylene-3,4,9,10-tetracarboxylic dianhydride (PTCDA) as a suitable organic cathode for full-cell evaluation.[29,39,40] For the cell assembly, we prepared the electrolyte-infiltrated organic cathode composite using the

https://doi.org/10.1021/acsenergylett.6c00026
ACS Energy Lett. XXXX, XXX, XXX−XXX

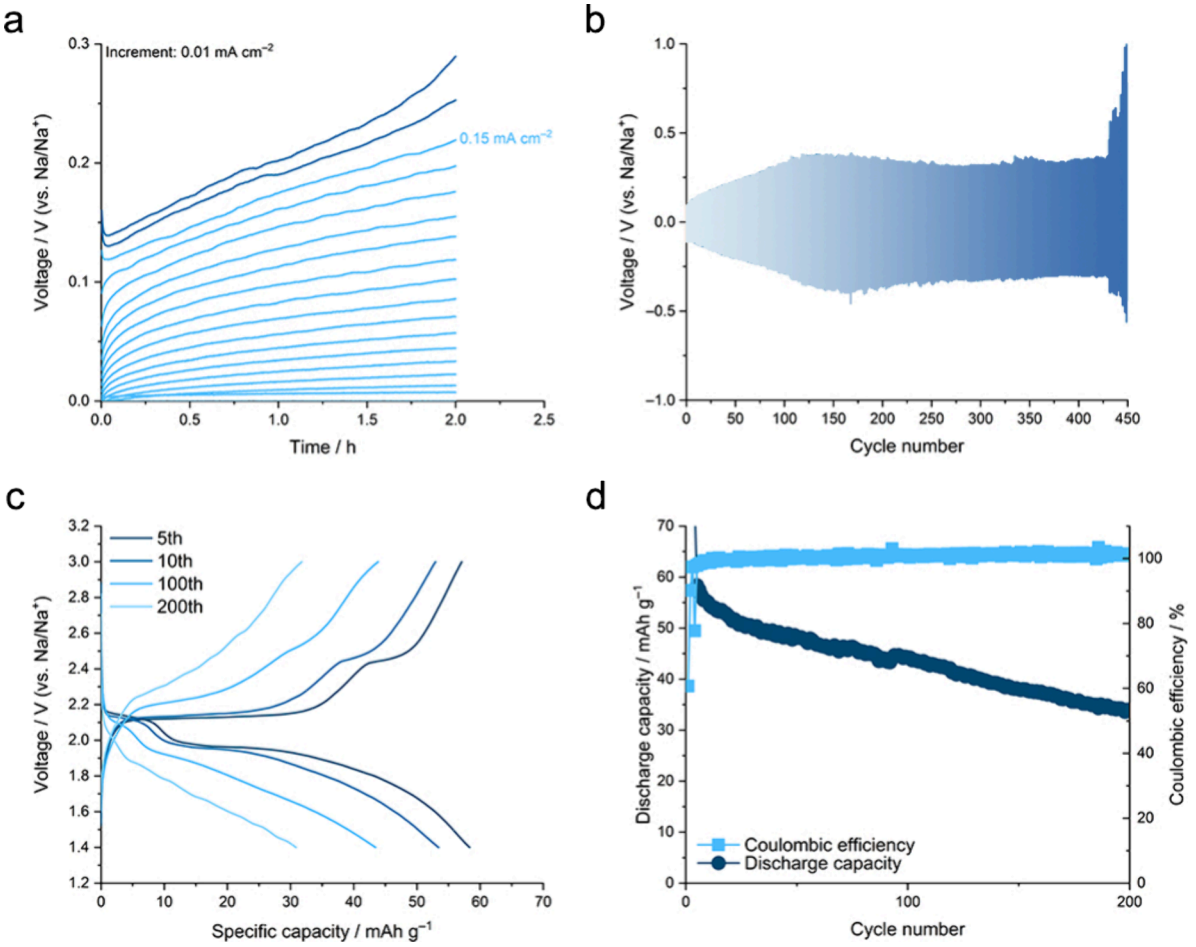

Figure 4. (a) Critical current density determination and (b) galvanostatic cycling of solid-state NaIORION electrolyte and Na symmetric cells operating at 60 °C. (c) Voltage profiles and (d) cycle-to-cycle performance of solid-state NaIORIONIcathode full cells operating at 60 °C.

procedure illustrated in Figure 1a, enabled by the thermoformability of Na ORION electrolyte and the wettability of the porous organic cathode. Infiltration of the ORION electrolyte has been examined with SEM analysis after FIB milling (Figure S16). Cathode composites exhibited porous morphologies before ORION electrolyte infiltration. However, the void space was filled with ORION electrolyte after infiltration, producing conformal cathode−electrolyte composites. This conformal contact was maintained after discharge and charge, enabling stable cycling of SSB. Full cells delivered an initial specific capacity of ∼60 mAh g^{-1} after formation and thereafter delivered stable cycling over 200 cycles with high Coulombic efficiency (Figure 4c,d). These results inform both the chemical and electrochemical compatibility of ORION electrolytes with organic cathodes and their ability to enable reversible redox reactions in a solid-state configuration. Furthermore, our work demonstrates the feasibility of solid-state battery fabrication through phase-change materials.

The emerging perspective stemming from our work is that both the thermoformability and favorable ion-transporting properties of ORION conductors require coordinating ligands, where declustering of ions enabled thereby lowers dramatically drops glass transition temperatures even in low prescribed amounts, speeds up ion dynamics, and increases ion mobility—without substantially changing the ratio of mobile vs structural ions. Instead, the additional ligand introduced fundamentally changes the way ions move through organo−ionic solids. Ligand-separated ion-pairs are the resting state for the mobile charge carriers in the system, and the ease in which those can be separated to support the ion current via vehicular motion guides ligand choices and stoichiometry, both here and in future designs. Critically, it does not appear necessary to add more ligand than available coordination sites for "liquid-like" ion transporting properties to emerge. This serves to maintain close ties between developments of concentrated liquid and solid electrolytes, the latter being the domain of the ORION electrolytes. ORION electrolytes also open the door to fundamental and practical comparisons of organic vs inorganic electrolytes and cathode materials in solid-state sodium metal batteries and likely other chemistries.

■ ASSOCIATED CONTENT

Data Availability Statement

All the data in this manuscript and Supporting Information are available upon reasonable request.

Supporting Information

The Supporting Information is available free of charge at https://pubs.acs.org/doi/10.1021/acsenergylett.6c00026.

Materials information, synthesis protocols, material characterization methods, electrochemical characterization, DSC, XRD, photos of ORION electrolyte homogenization tests, photos of ORION electrolyte

https://doi.org/10.1021/acsenergylett.6c00026
ACS Energy Lett. XXXX, XXX, XXX−XXX

thermoformability, Raman spectroscopy, NMR spectroscopy, impedance evolution, and LSV (PDF)

AUTHOR INFORMATION

Corresponding Author

Brett A. Helms − *The Molecular Foundry, Lawrence Berkeley National Laboratory, Berkeley, California 94720, United States; Energy Storage Research Alliance, Argonne National Laboratory, Lemont, Illinois 60439, United States; Materials Sciences Division, Lawrence Berkeley National Laboratory, Berkeley, California 94720, United States;* orcid.org/0000-0003-3925-4174; Email: bahelms@lbl.gov

Authors

Dong-Min Kim − *The Molecular Foundry, Lawrence Berkeley National Laboratory, Berkeley, California 94720, United States; Energy Storage Research Alliance, Argonne National Laboratory, Lemont, Illinois 60439, United States*

Gan Chen − *The Molecular Foundry, Lawrence Berkeley National Laboratory, Berkeley, California 94720, United States; Energy Storage Research Alliance, Argonne National Laboratory, Lemont, Illinois 60439, United States;* orcid.org/0000-0001-5541-6212

Michael A. Baird − *Department of Chemistry, University of California, Berkeley, California 94720, United States;* Present Address: Department of Chemical Engineering, Stanford University, Stanford, CA, 94305, U.S.A. (M.A.B.)

Livia Pugens Matte − *Energy Storage Research Alliance, Argonne National Laboratory, Lemont, Illinois 60439, United States; National Center for Electron Microscopy, Molecular Foundry, Lawrence Berkeley National Laboratory, Berkeley, California 94720, United States; Department of Materials Science and Engineering, University of California Berkeley, Berkeley, California 94720, United States*

Youngmin Ko − *The Molecular Foundry, Lawrence Berkeley National Laboratory, Berkeley, California 94720, United States;* Present Address: Department of Chemistry, Sungkyunkwan University, Suwon, 16419, Republic of Korea (Y.K.).

Carson O. Zellmann-Parrotta − *The Molecular Foundry, Lawrence Berkeley National Laboratory, Berkeley, California 94720, United States; Energy Storage Research Alliance, Argonne National Laboratory, Lemont, Illinois 60439, United States*

Jiwoong Bae − *The Molecular Foundry, Lawrence Berkeley National Laboratory, Berkeley, California 94720, United States;* Present Address: Department of Mechanical Engineering, Hanyang University, Seoul, 04763, Republic of Korea (J.B.).; orcid.org/0000-0003-0759-908X

Zhaoyang Chen − *Energy Storage Research Alliance, Argonne National Laboratory, Lemont, Illinois 60439, United States; Department of Electrical and Computer Engineering, University of Houston, Houston, Texas 77204, United States; Texas Center for Superconductivity at the University of Houston (TcSUH), University of Houston, Houston, Texas 77204, United States*

Yan Yao − *Energy Storage Research Alliance, Argonne National Laboratory, Lemont, Illinois 60439, United States; Department of Electrical and Computer Engineering, University of Houston, Houston, Texas 77204, United States; Texas Center for Superconductivity at the University of Houston (TcSUH), University of Houston, Houston, Texas 77204, United States*

Mary C. Scott − *Energy Storage Research Alliance, Argonne National Laboratory, Lemont, Illinois 60439, United States; National Center for Electron Microscopy, Molecular Foundry, Lawrence Berkeley National Laboratory, Berkeley, California 94720, United States; Department of Materials Science and Engineering, University of California Berkeley, Berkeley, California 94720, United States*

Ying Chen − *Energy Storage Research Alliance, Argonne National Laboratory, Lemont, Illinois 60439, United States; Physical and Computational Sciences Directorate, Pacific Northwest National Laboratory, Richland, Washington 99352, United States;* orcid.org/0000-0001-7417-0991

Complete contact information is available at: https://pubs.acs.org/10.1021/acsenergylett.6c00026

Notes

The authors declare the following competing financial interest(s): Y.Y. has equity interest in LiBeyond, LLC and Solid Design Instruments, LLC. The University of Houston reviewed and approved his relationship in compliance with its conflict-of-interest policy. B.A.H. has a financial interest in Cyklos Materials and Sepion Technologies. The other authors declare no competing financial interest.

ACKNOWLEDGMENTS

This work is funded by the Energy Storage Research Alliance "ESRA" (DE-AC02-06CH11357), an Energy Innovation Hub funded by the U.S. Department of Energy, Office of Science, Basic Energy Sciences. Work at the Molecular Foundry (XRD and FIB-SEM) was supported by the Office of Science, Office of Basic Energy Sciences, of the U.S. Department of Energy under Contract No. DE-AC02-05CH11231.

REFERENCES

(1) Ridley, P.; Nguyen, L. H. B.; Sebti, E.; Han, B.; Duong, G.; Chen, Y.-T.; Sayahpour, B.; Cronk, A.; Deysher, G.; Ham, S.-Y.; et al. Amorphous and nanocrystalline halide solid electrolytes with enhanced sodium-ion conductivity. *Matter* **2024**, *7* (2), 485−499.

(2) Radjendirane, A. C.; Maurya, D. K.; Ren, J.; Hou, H.; Algadi, H.; Xu, B. B.; Guo, Z.; Angaiah, S. Overview of Inorganic Electrolytes for All-Solid-State Sodium Batteries. *Langmuir* **2024**, *40* (32), 16690−16712.

(3) An, H.; Li, M.; Liu, Q.; Song, Y.; Deng, B.; Liu, X.; Wang, J. Hybrid electrolyte enables solid-state sodium batteries sustaining 50,000 cycles. *Nat. Sustain.* **2025**, *8* (6), 661−671.

(4) Jaschin, P. W.; Tang, C. R.; Wachsman, E. D. Fast Charging and Low Temperature Capabilities of Sodium Solid-State Batteries Enabled by Thin NASICON Bilayer Architecture. *ACS Energy Lett.* **2025**, *10* (6), 2610−2616.

(5) Deysher, G.; Oh, J. A. S.; Chen, Y.-T.; Sayahpour, B.; Ham, S.-Y.; Cheng, D.; Ridley, P.; Cronk, A.; Lin, S. W.-H.; Qian, K.; et al. Design principles for enabling an anode-free sodium all-solid-state battery. *Nat. Energy* **2024**, *9* (9), 1161−1172.

(6) Xiao, Y.; Wang, Y.; Bo, S.-H.; Kim, J. C.; Miara, L. J.; Ceder, G. Understanding interface stability in solid-state batteries. *Nat. Rev. Mater.* **2020**, *5* (2), 105−126.

(7) Si, H.; Ma, J.; Xia, X.; Wang, Q.; Geng, S.; Fu, L. Solid-State Sodium-Ion Batteries: Theories, Challenges and Perspectives. *Chem.—Eur. J.* **2025**, *31* (5), No. e202403247.

(8) Lou, S.; Zhang, F.; Fu, C.; Chen, M.; Ma, Y.; Yin, G.; Wang, J. Interface Issues and Challenges in All-Solid-State Batteries: Lithium, Sodium, and Beyond. *Adv. Mater.* **2021**, *33* (6), 2000721.

(9) Cheng, L.; Crumlin, E. J.; Chen, W.; Qiao, R.; Hou, H.; Franz Lux, S.; Zorba, V.; Russo, R.; Kostecki, R.; Liu, Z.; et al. The origin of high electrolyte-electrode interfacial resistances in lithium cells containing garnet type solid electrolytes. *Phys. Chem. Chem. Phys.* **2014**, *16* (34), 18294−18300.
(10) Pervez, S. A.; Cambaz, M. A.; Thangadurai, V.; Fichtner, M. Interface in Solid-State Lithium Battery: Challenges, Progress, and Outlook. *ACS Appl. Mater. Interfaces* **2019**, *11* (25), 22029−22050.
(11) Vardar, G.; Bowman, W. J.; Lu, Q.; Wang, J.; Chater, R. J.; Aguadero, A.; Seibert, R.; Terry, J.; Hunt, A.; Waluyo, I.; et al. Structure, Chemistry, and Charge Transfer Resistance of the Interface between Li7La3Zr2O12 Electrolyte and LiCoO2 Cathode. *Chem. Mater.* **2018**, *30* (18), 6259−6276.
(12) Feng, X.; Fang, H.; Wu, N.; Liu, P.; Jena, P.; Nanda, J.; Mitlin, D. Review of modification strategies in emerging inorganic solid-state electrolytes for lithium, sodium, and potassium batteries. *Joule* **2022**, *6* (3), 543−587.
(13) Kim, K. J.; Rupp, J. L. M. All ceramic cathode composite design and manufacturing towards low interfacial resistance for garnet-based solid-state lithium batteries. *Energy Environ. Sci.* **2020**, *13* (12), 4930−4945.
(14) Kong, X.; Gu, R.; Jin, Z.; Zhang, L.; Zhang, C.; Xiang, W.; Li, C.; Zhu, K.; Xu, Y.; Huang, H.; et al. Maximizing interface stability in all-solid-state lithium batteries through entropy stabilization and fast kinetics. *Nat. Commun.* **2024**, *15* (1), 7247.
(15) Puls, S.; Nazmutdinova, E.; Kalyk, F.; Woolley, H. M.; Thomsen, J. F.; Cheng, Z.; Fauchier-Magnan, A.; Gautam, A.; Gockeln, M.; Ham, S.-Y.; et al. Benchmarking the reproducibility of all-solid-state battery cell performance. *Nat. Energy* **2024**, *9* (10), 1310−1320.
(16) Cronau, M.; Szabo, M.; König, C.; Wassermann, T. B.; Roling, B. How to Measure a Reliable Ionic Conductivity? The Stack Pressure Dilemma of Microcrystalline Sulfide-Based Solid Electrolytes. *ACS Energy Lett.* **2021**, *6* (9), 3072−3077.
(17) Doux, J.-M.; Nguyen, H.; Tan, D. H. S.; Banerjee, A.; Wang, X.; Wu, E. A.; Jo, C.; Yang, H.; Meng, Y. S. Stack Pressure Considerations for Room-Temperature All-Solid-State Lithium Metal Batteries. *Adv. Energy Mater.* **2020**, *10* (1), 1903253.
(18) Wu, Z.; He, S.; Zheng, C.; Gan, J.; She, L.; Zhang, M.; Gao, Y.; Yang, Y.; Pan, H. Fabrication pressures and stack pressures in solid-state battery. *eScience* **2024**, *4* (4), 100247.
(19) Ihrig, M.; Finsterbusch, M.; Laptev, A. M.; Tu, C.-h.; Tran, N. T. T.; Lin, C.-a.; Kuo, L.-Y.; Ye, R.; Sohn, Y. J.; Kaghazchi, P.; et al. Study of LiCoO2/Li7La3Zr2O12:Ta Interface Degradation in All-Solid-State Lithium Batteries. *ACS Appl. Mater. Interfaces* **2022**, *14* (9), 11288−11299.
(20) Yao, K.; Scheld, W. S.; Ma, Q.; Zeng, Y.; Ganapathy, S.; Ihrig, M.; Ye, R.; Ma, M.; Kiyek, V.; Guillon, O.; et al. Holistic view on cation interdiffusion during processing and operation of garnet all-solid-state batteries. *Energy Storage Mater.* **2024**, *71*, 103662.
(21) Kim, K. H.; Iriyama, Y.; Yamamoto, K.; Kumazaki, S.; Asaka, T.; Tanabe, K.; Fisher, C. A. J.; Hirayama, T.; Murugan, R.; Ogumi, Z. Characterization of the interface between LiCoO2 and Li7La3Zr2O12 in an all-solid-state rechargeable lithium battery. *J. Power Sources* **2011**, *196* (2), 764−767.
(22) Kim, Y.; Kim, D.; Bliem, R.; Vardar, G.; Waluyo, I.; Hunt, A.; Wright, J. T.; Katsoudas, J. P.; Yildiz, B. Thermally Driven Interfacial Degradation between Li7La3Zr2O12 Electrolyte and LiNi0.6Mn0.2Co0.2O2 Cathode. *Chem. Mater.* **2020**, *32* (22), 9531−9541.
(23) Richards, W. D.; Miara, L. J.; Wang, Y.; Kim, J. C.; Ceder, G. Interface Stability in Solid-State Batteries. *Chem. Mater.* **2016**, *28* (1), 266−273.
(24) Clausnitzer, M.; Ihrig, M.; Cressa, L.; Hein, S.; Finsterbusch, M.; Eswara, S.; Kuo, L.-Y.; Danner, T.; Kaghazchi, P.; Fattakhova-Rohlfing, D.; et al. Impact of degradation mechanisms at the cathode/electrolyte interface of garnet-based all-solid-state batteries. *Energy Storage Mater.* **2024**, *67*, 103262.
(25) Kalnaus, S.; Dudney, N. J.; Westover, A. S.; Herbert, E.; Hackney, S. Solid-state batteries: The critical role of mechanics. *Science* **2023**, *381* (6664), No. eabg5998.
(26) Bucci, G.; Talamini, B.; Renuka Balakrishna, A.; Chiang, Y.-M.; Carter, W. C. Mechanical instability of electrode-electrolyte interfaces in solid-state batteries. *Phys. Rev. Mater.* **2018**, *2* (10), 105407.
(27) Barai, P.; Rojas, T.; Narayanan, B.; Ngo, A. T.; Curtiss, L. A.; Srinivasan, V. Investigation of Delamination-Induced Performance Decay at the Cathode/LLZO Interface. *Chem. Mater.* **2021**, *33* (14), 5527−5541.
(28) Bae, J.; Zhu, Z.; Yan, J.; Kim, D.-M.; Ko, Y.; Jain, A.; Helms, B. A. Closed-loop cathode recycling in solid-state batteries enabled by supramolecular electrolytes. *Sci.Adv.* **2023**, *9* (32), No. eadh9020.
(29) Yang, S.; Shao, C.; Xiao, X.; Fang, D.; Li, N.; Zhao, E.; Wang, C.; Chen, L.; Li, N.; Li, J.; et al. Revealing stable organic cathode/solid electrolyte interface to promote all-solid-state sodium batteries using organic cathodes. *Energy Storage Mater.* **2024**, *73*, 103857.
(30) Yamada, Y.; Wang, J.; Ko, S.; Watanabe, E.; Yamada, A. Advances and issues in developing salt-concentrated battery electrolytes. *Nat. Energy* **2019**, *4* (4), 269−280.
(31) Xiang, J.; Lu, Y.-C. Ether-Based High-Voltage Lithium Metal Batteries: The Road to Commercialization. *ACS Nano* **2024**, *18* (16), 10726−10737.
(32) Li, Z.; Rao, H.; Atwi, R.; Sivakumar, B. M.; Gwalani, B.; Gray, S.; Han, K. S.; Everett, T. A.; Ajantiwalay, T. A.; Murugesan, V.; et al. Non-polar ether-based electrolyte solutions for stable high-voltage non-aqueous lithium metal batteries. *Nat. Commun.* **2023**, *14* (1), 868.
(33) Zheng, J.; Chen, S.; Zhao, W.; Song, J.; Engelhard, M. H.; Zhang, J.-G. Extremely Stable Sodium Metal Batteries Enabled by Localized High-Concentration Electrolytes. *ACS Energy Lett.* **2018**, *3* (2), 315−321.
(34) Takada, K.; Yamada, Y.; Watanabe, E.; Wang, J.; Sodeyama, K.; Tateyama, Y.; Hirata, K.; Kawase, T.; Yamada, A. Unusual Passivation Ability of Superconcentrated Electrolytes toward Hard Carbon Negative Electrodes in Sodium-Ion Batteries. *ACS Appl. Mater. Interfaces* **2017**, *9* (39), 33802−33809.
(35) Ke, J.; Kim, Y.; Su, L. Localized High-Concentration Electrolytes for Sodium Batteries: Fundamentals, Challenges, and Applications. *ACS Appl. Energy Mater.* **2025**, *8* (13), 8850−8861.
(36) Wang, J.; Yamada, Y.; Sodeyama, K.; Chiang, C. H.; Tateyama, Y.; Yamada, A. Superconcentrated electrolytes for a high-voltage lithium-ion battery. *Nat. Commun.* **2016**, *7* (1), 12032.
(37) Jiao, S.; Ren, X.; Cao, R.; Engelhard, M. H.; Liu, Y.; Hu, D.; Mei, D.; Zheng, J.; Zhao, W.; Li, Q.; et al. Stable cycling of high-voltage lithium metal batteries in ether electrolytes. *Nat. Energy* **2018**, *3* (9), 739−746.
(38) Chen, W.; Park, J.-S.; Kwon, C.; Plaza-Rivera, C. O.; Hsu, C.-W.; Phong, J. K.; Kilgallon, L. J.; Wang, D.; Dai, T.; Kim, S. Y.; et al. Hybrid solvating electrolytes for practical sodium-metal batteries. *Joule* **2025**, *9* (3), 101811.
(39) Zhu, Y.; Guo, X.; Thomas, S.; Yin, J.; Yuan, Y.; Tian, Z.; Harrison, G. T.; De Wolf, S.; Bakr, O. M.; Mohammed, O. F.; et al. An ultrafast Na-ion battery chemistry through coupling sustainable organic electrodes with modulated aqueous electrolytes. *Energy Environ. Sci.* **2024**, *17* (7), 2480−2491.
(40) Luo, W.; Allen, M.; Raju, V.; Ji, X. An Organic Pigment as a High-Performance Cathode for Sodium-Ion Batteries. *Adv. Energy Mater.* **2014**, *4* (15), 1400554.

https://doi.org/10.1021/acsenergylett.6c00026
ACS Energy Lett. XXXX, XXX, XXX−XXX